Journal Pre-proof

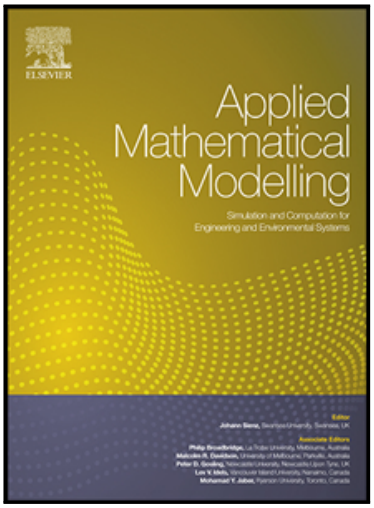

Computational design of thermo-mechanical metadevices using topology optimization

Juan C. Álvarez Hostos, Víctor D. Fachinotti, Ignacio Peralta

PII: S0307-904X(20)30550-3
DOI: https://doi.org/10.1016/j.apm.2020.09.030
Reference: APM 13682

To appear in: *Applied Mathematical Modelling*

Received date: 24 September 2019
Revised date: 15 August 2020
Accepted date: 9 September 2020

Please cite this article as: Juan C. Álvarez Hostos, Víctor D. Fachinotti, Ignacio Peralta, Computational design of thermo-mechanical metadevices using topology optimization, *Applied Mathematical Modelling* (2020), doi: https://doi.org/10.1016/j.apm.2020.09.030

Centro de Investigación de
Métodos Computacionales

Universidad Nacional del Litoral
Consejo Nacional de Investigaciones
Científicas y Técnicas

Santa Fe, September 24th 2019

Highlights

- Topology optimization-based design of thermo-mechanical metadevices is proposed
- The so-designed devices can be manufactured by using simple isotropic materials
- The devices performance has been analyzed via finite element method simulations
- Such devices exhibit a good performance, when compared to more complex metadevices

CIMEC (UNL/CONICET)
Predio CONICET-Santa Fe
Colectora Ruta Nac. 168 / Paraje El Pozo
3000 Santa Fe - Argentina

Tel: +54-342- 451 1594 / 95 x 7045
Fax: +54-342- 451 1169
e-mail: jchostos@cimec.unl.edu.ar

Computational design of thermo-mechanical metadevices using topology optimization

Juan C. Álvarez Hostos[*,a,b], Víctor D. Fachinotti[a] and Ignacio Peralta[a,c]

[a]Centro de Investigación de Métodos Computacionales (CIMEC), Universidad Nacional del Litoral (UNL)/Consejo Nacional de Investigaciones Científicas y Técnicas (CONICET), Predio CCT-CONICET Santa Fe, Argentina.
[b]Department of Chemical Metallurgy, Universidad Central de Venezuela, Ciudad Universitaria, Los Chaguaramos, Caracas, Venezuela.
[c]Laboratorio de Flujometra (FLOW), Facultad Regional Santa Fe (FRSF), Universidad Tecnolgica Nacional (UTN), Lavaise 610, 3000, Santa Fe, Argentina.

Abstract

The present work has been conducted in order to introduce a novel approach for the design of mechanical devices conceived to manipulate the displacements field in linear elastic materials subjected to thermal gradients. Such an approach involves the solution of a topology optimization problem where the objective function defines the error in achieving a prescribed displacement field, and the mechanical device consists of two macroscopically distinguishable isotropic candidate materials. The material distribution is defined as a continuous function by following the solid isotropic microstructure (or material) with penalization (SIMP) method. The so-designed devices are easy to manufacture, since the design variables dictate the candidate materials distribution. Based on such an approach it is not necessary to devise further ways to simultaneously mimicking several thermal and mechanical effective properties, as required by coordinates transformation-based metamaterial design methods. Although the candidate materials are isotropic, the mechanical device behaves as a metamaterial allowing the desired manipulation of the displacements field. As an example, this topology optimization-based approach is applied to the design of an elastostatic cloaking device subjected to thermal gradients, considering also thermo-dependent mechanical properties.

Keywords: Topology Optimization, Metadevices, Thermo-mechanical, Cloaking, Sensitivity Analysis, Design Variables

1. Introduction

Recent developments in engineered materials has allowed the manipulation of physical fields in outstanding and unprecedented ways, including cloaking [1–6], concentration [2, 4, 6–11], inversion [4, 6–8], shielding [4–6] and channeling [6, 12] in heat conduction, and cloaking in elastostatics [13–16], elastodynamics [17–19] and acoustics [20], among others. These engineered materials are called metamaterials for having effective properties that goes beyond (meta in Greek) those found in nature.

Classically, metamaterials and metadevices (those devices made of or behaving as metamaterials) have been designed via the coordinate transformation approach originally proposed by Leonhardt [21] and Pendry [22] for electromagnetic cloaking. Such an idea was subsequently adapted to the design of metadevices for heat flux manipulation [1–3, 9] and mechanical cloaking [18, 19]. The implementation of such an approach in the design of mechanical metamaterials leads to the need of achieving an invariant form of the linear momentum balance equation, which poses several issues. Norris and Shuvalov [23] demonstrated that the coordinates transformation procedure leads to the anisotropic materials obeying the Willis constitutive equations [24]. Milton et al. [25] achieved a transformation-invariant form of the linear momentum balance for cloaking by including a third-order tensor besides the standard (fourth-order) elasticity tensor, whereas Brun et al. [26] did it by breaking the symmetry of the standard elasticity tensor. Great efforts have been devoted to manufacture the so-conceived mechanical metamaterials [13, 14, 17, 27]. Stenger et al. [17] designed a circular mechanical cloaking device with radially variable effective elastic properties, in an attempt to emulate the invariant form of the plate equation derived by Farhat et al. [28]. Kadic et al. [27] proposed to use pentamodal materials to emulate any material conceived from coordinates transformation, and such an idea was followed by Bückmann et al. [13] for the manufacture of an elastostatic cloaking device. As an alternative to the coordinates transformation-based procedures, Bückmann et al. [14] proposed the implementation of a direct-lattice transformation technique to design elastostatic cloaking devices. Such an approach is conceived to directly prescribe the geometry of the metamaterial or metadevice to be manufactured from lattices without the need of devising further ways to achieve the inhomogeneous material properties required for the task accomplishment, which is a crucial improvement in comparison with the coordinates transformation-based procedure.

Recently, Peralta et al. [10] introduced the optimization-based metamaterial design (OMD) approach for the design of thermal metamaterials, free from the limitations of coordinates transformation-based procedures. Such a procedure consists in solving a large-scale continuous optimization problem to minimize the error in the accomplishment of a given task, where the parameters describing the metamaterial microstructure (microparameters) are taken as design variables. Examples of design variables are the geometrical parameters defining a biomimetic unit cell of artificial bones [29, 30], the relative thickness of layers and their orientation in laminates [5, 10, 16], and the artificial density [31, 32] in material distribution problems. Like the direct-lattice technique [14], the OMD approach directly prescribes how

to manufacture the metamaterial or metadevice. Additionally, it allows the design of any metadevice having a quantitatively characterizable microstructure, including lattices as particular cases. Another noteworthy advantage of the OMD approach lies on the possibility of designing metadevices conceived to perform any heat flux manipulation task (including concentration, shielding, reversion, and cloaking), by using a unique objective function to avoid the need of a different formulation for each task [4]. The OMD versatility was demonstrated when it was extended to the design of metadevices for elastostatic cloaking under given boundary traction [15] and thermal gradients [16].

Although OMD dictates how to manufacture the metamaterial at each point, the achievement of such a precise inhomogeneous metamaterial is still a critical issue that precludes real applications. In further efforts towards manufacturability, the well known topology optimization method [33] was used in the design of thermal [4, 11], mechanical [15], and thermo-mechanical [31, 32, 34–38] metadevices. Topology optimization was originally formulated for structural problems [39–41], where the design variables define the presence of material at a point. According to the possibility of achieving a discrete material distribution in terms of continuous design variables, this technique has been successfully extended to heat transfer [42, 43], electro-mechanical [44], fluid flow [45], dynamic fatigue [46, 47], thermo-mechanical [48, 49] and even electro-thermo-mechanical [50] applications. Regarding the design of metamaterials and metadevices, the design variables are rather used to choose between materials with highly contrasting properties. Topology optimization-based metamaterial design (TOMD) has changed the mainstream belief that it is imperative to use anisotropic inhomogeneous metamaterials for the manipulation of macroscopic fields [7, 14, 18, 51]. For instance, Fachinotti et al. [4] applied the well-known solid isotropic microstructure (or material) with penalization (SIMP) [33] approach in the framework of TOMD in order to design an easy-to-make heat flux inversion metadevice, which consisted of two piecewise macroscopically distinguishable homogeneous materials with very different isotropic thermal conductivities. Such a device was actually significantly simpler, easier to make and more efficient than the coordinates transformation-based inverter designed by Narayana and Sato [51]. Sigmund and Torquato [31, 32] used TOMD with a SIMP-like approach involving three phases (two solids, one void) to optimize both the topology and material distribution in each base cell of metamaterials for extreme thermal expansion responses, whereas Wang et al. [34, 36, 37] used a multiphase level-set method for such a purpose. The possibility of manufacturing such thermo-mechanical metamaterials obtained by TOMD has been demonstrated by Takezawa et al. [35], who have succeeded in implementing additive manufacturing techniques to obtain an extreme thermal expansion metamaterial designed via a SIMP-based multiphase topology optimization procedure [31, 32] coupled to a phase field method [52].

Later, Peralta et al. [11] adapted a multiphase topology optimization method known as discrete material optimization (DMO) [53] to the design of thermal metadevices made of any number of homogeneous candidate materials, either isotropic or not. By this way, these authors designed a heat flux concentrator made of laminates of copper and polydimethylsiloxane in different orientations. As a further demonstration of its versatility, this approach was applied by Fachinotti et al. [15] for the design of mechanical metadevices, showing an elastostatic cloaking device as example.

Regarding all the previously mentioned TOMD-based thermo-mechanical metamaterials for extreme thermal expansion [31, 32, 34–38], it is worth to mention that such metamaterials were conceived under the assumption that the temperature is homogeneous throughout the metamaterial without being affected by the material distribution. Such an excessively restrictive hypothesis is actually appropriate only when a unique temperature is prescribed on all the device boundaries and there are no internal heat sources, given the usually high conductivity contrast within metamaterials. The sensitivity of coupled temperature and displacement fields to microstructural changes [54] has been recently accounted for Álvarez-Hostos et al. [16] in the design of thermo-mechanical metamaterials, which involves the coupled solution of heat transfer and mechanical problems throughout the entire optimization process. These authors used the OMD approach, hence suffering from manufacturability issues.

In agreement with the aforementioned aspects, the present work is focused on extending the TOMD approach (and its advantages regarding manufacturability) to the design of thermo-mechanical metadevices accounting for the coupling between displacement and temperature fields. In this case, the objective function representing the mechanical task (e.g., elastostatic cloaking) will depend on displacement, which in turn depends on temperature. Accordingly, the performance of such metadevices will be dictated by the spatial distribution of both mechanical (elastic moduli and thermal expansion) and transport (conductivity) properties, which are dependent on the design variables defining the material distribution in the optimization problem. So, the computation of the objective function at each one of the iterations (usually, hundreds to thousands) during the optimization process requires the fully coupled solution of the linear momentum and thermal energy balance equations, making this thermo-mechanical problem considerably more expensive to solve when compared to that in which a homogeneous temperature field is directly prescribed [31, 32, 34–38].

The current TOMD is conducted under the classical SIMP approach [33] for the design of thermo-mechanical metadevices, which consist of two piecewise macroscopically distinguishable homogeneous materials with very different mechanical (elastic moduli and thermal expansion coefficient) and thermal (conductivity) properties. As a

further contribution unprecedented in the design of thermo-mechanical metamaterials and metadevices, the dependence of elastic moduli with the temperature is allowed.

Finally, a device for cloaking under surface traction and thermal gradients is designed using two isotropic materials (aluminum and polyethylene) in order to highlight the capability of this approach to design easy-to-make thermo-mechanical metadevices. The performance of such a cloaking metadevice of feasible manufacture can actually be compared to that of a metamaterial proposed in a previous communication [16], which is made of laminates based on the same materials. Such metamaterial consists in an inhomogeneous distribution of the relative thickness of the constituent materials and orientation of the laminates, whereby its manufacturability is uncertain.

2. Governing equations

The topology optimization-based design of a thermo-mechanical metadevice implies the minimization of an objective function that quantifies the error in accomplishing a given task, which generally depends on displacement and temperature. The evaluation of such an objective function requires to solve both the linear momentum and thermal energy balance equations, which is done in this work via the finite element method (FEM).

2.1. Thermo-mechanical problem

The domain Ω depicted in Fig. 1 represents a heterogeneous solid body, undergoing a steady state thermo-mechanical loading process. Assuming a linear thermo-elastic behaviour and small strains, the displacement field $\mathbf{u}$ in Ω is governed by the equilibrium equation:

$$\operatorname{div}\boldsymbol{\sigma} + \mathbf{b} = \mathbf{0}, \tag{1}$$

where $\mathbf{b}$ is the body force, and $\boldsymbol{\sigma}$ is the Cauchy stress tensor defined by the Duhamel-Neumann law for thermo-elasticity:

$$\boldsymbol{\sigma} = \mathbf{C} : \boldsymbol{\varepsilon} + \mathbf{d}\,(T - T_{\text{ref}})\,,$$

being $\boldsymbol{\varepsilon} = [\operatorname{grad}\mathbf{u} + (\operatorname{grad}\mathbf{u})^T]/2$ the infinitesimal strain tensor, $\mathbf{C}$ the elastic moduli tensor, $\mathbf{d}$ the stress increment per unit temperature, T the temperature and T_{ref} the reference temperature for zero thermal strain. The solution of Eq. (1) is subjected to the boundary conditions:

$$\begin{aligned} \mathbf{u} &= \mathbf{u}^{\text{wall}} && \text{in } \Gamma_{\mathbf{u}}, \\ \boldsymbol{\sigma}\cdot\mathbf{n} &= \mathbf{t}^{\text{wall}} && \text{in } \Gamma_{\mathbf{t}}, \end{aligned}$$

where $\mathbf{n}$ is the unit vector normal to and pointing outwards Γ, whereas $\mathbf{u}^{\text{wall}}$ and $\mathbf{t}^{\text{wall}}$ are the displacement and surface traction vectors prescribed on the non overlapping portions $\Gamma_{\mathbf{u}}$ and $\Gamma_{\mathbf{t}}$ of Γ, respectively.

The dependence of $\mathbf{u}$ on T gives rise to the need of coupling the solution of (1) to the heat conduction equation:

$$-\operatorname{div}(\mathbf{q}) + s = 0, \tag{2}$$

where s is the internal heat source, and $\mathbf{q}$ the heat flux vector given by the Fourier's Law.

$$\mathbf{q} = -\mathbf{k}\cdot\operatorname{grad} T,$$

being $\mathbf{k}$ the thermal conductivity tensor. The solution of Eq. (2) is subjected to the boundary conditions:

$$\begin{aligned} T &= T^{\text{wall}} && \text{in } \Gamma_T, \\ \mathbf{q}\cdot\mathbf{n} &= q^{\text{wall}} && \text{in } \Gamma_q, \end{aligned}$$

where T^{wall} and q^{wall} are the temperature and heat flux prescribed on the non overlapping portions Γ_T and Γ_q of Γ, respectively.

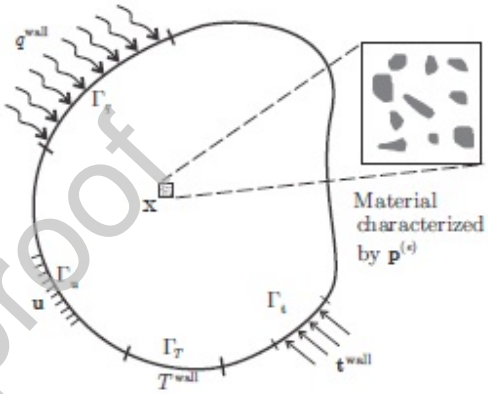

Figure 1: Thermo-mechanical problem in a macroscopic domain where the effective properties depend on a quantitatively characterized microstructure

2.2. Finite element formulation

The thermo-mechanical problem described in the previous section will be solved by using the FEM with Ω divided in finite elements $\Omega^{(e)}$, and approximating the temperature and displacement fields for all $\mathbf{x} \in \Omega$ as follows:

$$T(\mathbf{x}) = N_i T_i = \mathbf{N}(\mathbf{x})\mathbf{T}, \tag{3}$$

$$\mathbf{u}(\mathbf{x}) = N_i \mathbf{u}_i = \mathbf{N}^{\text{m}}(\mathbf{x})\mathbf{U}, \tag{4}$$

where T_i and $\mathbf{u}_i$ are the temperature and displacement unknown at each node $\mathbf{x}_i$ of the finite element mesh, and N_i is the shape function associated to this node, for which $N_i(\mathbf{x}_j) = \delta_{ij}$ with δ_{ij} denoting the Kronecker delta. T_i and $\mathbf{u}_i$ are grouped in vectors $\mathbf{T}$ and $\mathbf{U}$, respectively. The shape functions N_i are grouped either in the row vector $\mathbf{N}$ and matrix $\mathbf{N}^{\text{m}}$ for the thermal and mechanical analysis, respectively. The substitution of Eq. (3) in the Bubnov-Galerkin weak-form of the thermal problem leads to:

$$\mathbf{K}\mathbf{T} = \mathbf{Q}, \tag{5}$$

with

$$\mathbf{K} = \int_\Omega \mathbf{B}^T\mathbf{k}\mathbf{B}\,\mathrm{d}\Omega, \tag{6}$$

$$\mathbf{Q} = \underbrace{\int_\Omega \mathbf{N}^T s\,\mathrm{d}\Omega}_{\mathbf{Q}^s} - \underbrace{\int_{\Gamma_q} \mathbf{N}^T q^{\text{wall}}\,\mathrm{d}\Gamma_q}_{\mathbf{Q}^q} \tag{7}$$

where $\mathbf{B}$ is the matrix of shape functions gradient with components $B_{ij} = \partial N_i/\partial X_j$. Similarly, the following system of equations is obtained after substituting Eq. (4) in the Bubnov-Galerkin weak-form of the mechanical problem:

$$\mathbf{K}^{\mathrm{m}}\mathbf{U} = \mathbf{F}, \tag{8}$$

with

$$\mathbf{K}^{\mathrm{m}} = \int_{\Omega} [\mathbf{B}^{\mathrm{m}}]^T \, \mathbf{C}\mathbf{B}^{\mathrm{m}} \mathrm{d}\Omega, \tag{9}$$

$$\mathbf{F} = \underbrace{\int_{\Gamma_t} \mathbf{N}^T \mathbf{t}^{\mathrm{wall}} \, \mathrm{d}\Gamma_{\mathbf{t}}}_{\mathbf{F^t}} + \underbrace{\int_{\Omega} \mathbf{N}^T \mathbf{b} \, \mathrm{d}\Omega}_{\mathbf{F^b}} - \underbrace{\int_{\Omega} [\mathbf{B}^{\mathrm{m}}]^T \, \mathbf{d} \, (T - T_{\mathrm{ref}}) \, \mathrm{d}\Omega}_{\mathbf{F}^{\mathrm{Th}}}, \tag{10}$$

where $\mathbf{B}^{\mathrm{m}}$ denotes the strain-displacement matrix. In Eqs. (9) and (10), the elastic moduli $\mathbf{C}$ and stress increment per unit temperature $\mathbf{d}$ tensors are given in Voigt notation. Let the microstructure at each finite element $\Omega^{(e)}$ in a heterogeneous region $\Omega_{\mathrm{dev}} \subset \Omega$ occupied by a metadevice, be quantitatively characterized by a vector $\mathbf{p}_e$ of M microparameters. Accordingly, the effective material properties $\mathbf{C}$, $\mathbf{d}$ and $\mathbf{k}$ at each $\Omega^{(e)} \in \Omega_{\mathrm{dev}}$ are function of $\mathbf{p}^{(e)}$. Consequently the global conduction $\mathbf{K}$ and stiffness $\mathbf{K}^{\mathrm{m}}$ matrices, and also the global thermal loads vector $\mathbf{F}^{\mathrm{Th}}$ are function of the microstructure distribution in Ω_{dev}:

$$\mathbf{K} = \mathbf{K}(\mathbf{P}), \quad \mathbf{K}^{\mathrm{m}} = \mathbf{K}^{\mathrm{m}}(\mathbf{P}), \quad \text{and} \quad \mathbf{F}^{\mathrm{Th}} = \mathbf{F}^{\mathrm{Th}}(\mathbf{P}),$$

with

$$\mathbf{P} = [\mathbf{p}^{(1)}, \mathbf{p}^{(2)}, ..., \mathbf{p}^{(N)}],$$

whereby both the displacement and thermal fields in the whole domain Ω depend on $\mathbf{P}$, i.e. $\mathbf{u} = \mathbf{u}(\mathbf{x}, \mathbf{P})$ and $T = T(\mathbf{x}, \mathbf{P})$ for all $\mathbf{x} \in \Omega$ [54].

2.3. The displacements manipulation problem under thermal loads

The problem of designing a metadevice Ω_{dev} embedded in the body Ω to manipulate the displacement inside the region $\Omega_{\mathrm{task}} \subset \Omega$ subjected to both thermal and mechanical loads, can be stated as follows: to find $\mathbf{P}$ such that

$$\mathbf{u}(\mathbf{x}, \mathbf{P}) = \bar{\mathbf{u}}(\mathbf{x}), \quad \text{for all } \mathbf{x} \in \Omega_{\mathrm{task}}, \tag{11}$$

where $\bar{\mathbf{u}}(\mathbf{x})$ is a prescribed displacement field to be achieved in a region $\Omega_{\mathrm{task}} \subset \Omega$. Given the link between the thermal and mechanical responses of the domain, the accomplishment of any displacements manipulation task requires to find a proper spatial distribution of both thermal and mechanical material properties. Thus, the fulfillment of such a task will be affected by the dependence of both displacement and temperature on the microparameters distribution.

In order to make feasible the numerical solution of this problem, the task accomplishment is checked at H points $\mathbf{x}^{(h)} \in \Omega_{\mathrm{task}}$. Further, to guarantee the microstructure feasibility, the search of $\mathbf{P}$ must be constrained to a feasible design set $\mathcal{D}$. Such a constraint precludes the perfect fulfillment of (11), and it is achieved up to a minimum error:

$$f(\mathbf{P}) = \left[\frac{\sum_{h=1}^{H} \left\| \mathbf{u}(\mathbf{x}^{(h)}, \mathbf{P}) - \bar{\mathbf{u}}(\mathbf{x}^{(h)}) \right\|^2}{\sum_{h=1}^{H} \left\| \bar{\mathbf{u}}(\mathbf{x}^{(h)}) \right\|^2} \right]^{1/2}, \tag{12}$$

where the relative error f in the accomplishment of the displacements manipulation task at all the points $\mathbf{x}^{(h)} \in \Omega_{\mathrm{task}}$ defines the objective function, whereas the microparameters P_i defining the microstructure distribution in Ω_{dev} are the design variables.

Constraining the search of $\mathbf{P}$ to a feasible design set $\mathcal{D}$ precludes the exact accomplishment of (11), which actually represents a near-elastostatic cloaking under thermal gradients. The near-cloaking problem in elastostatic has also recently been addressed by Craster et al. [55] through a different formulation, which is based on the regularized change of variable originally developed by Kohn et al. [56] for electromagnetic cloaking.

The optimization-based procedure proposed in this communication implies to solve the following non-linear constrained optimization problem:

$$\min_{\mathbf{P} \in \mathcal{D}} f(\mathbf{P}) \tag{13}$$

In principle, there are M design variables per finite element, whereby the optimization problem (13) is usually a large-scale problem. If the feasible design set $\mathcal{D}$ is rich enough, it would be possible to achieve a perfect design. If not, it is still possible to obtain a design for which (12) reaches a minimum. In a previous communication [16], the optimization-based approach has been successfully implemented in the design of thermo-mechanical metadevices by using a metamaterial consisting of an orthotropic composite laminate made of two materials with very different thermal and mechanical properties. In such study, there were $M = 2$ design variables (the relative thickness and orientation of the laminate) at each finite element in the metadevice. Such a design has been obtained without introducing manufacturability constraints, which have already been recognized to be crucial for the manufacture of both thermal [4, 11] and mechanical [15] metadevices. Therefore, the optimization-based design of the current thermo-mechanical metadevice will be conducted putting also special emphasis on manufacturability. Such a feature will be assured by following the SIMP approach, which has been widely used in topology optimization problems. In a previous work, such a technique was successfully implemented in the design of easy-to-make heat flux manipulation metadevices [4]. Thus, in this study the effective elastic moduli, stress increment per unit temperature and thermal conductivity at each finite element $\Omega^{(e)} \in \Omega_{\mathrm{dev}}$, are defined as:

$$\mathbf{C}^{(e)} = \rho_e^p \mathbf{C}_{\mathrm{A}} + (1 - \rho_e^p)\mathbf{C}_{\mathrm{B}},$$
$$\mathbf{d}^{(e)} = \rho_e^p \mathbf{d}_{\mathrm{A}} + (1 - \rho_e^p)\mathbf{d}_{\mathrm{B}},$$
$$\mathbf{k}^{(e)} = \rho_e^p \mathbf{k}_{\mathrm{A}} + (1 - \rho_e^p)\mathbf{k}_{\mathrm{B}},$$

where $p > 1$, ρ_e is an artificial density with $0 \leq \rho_e \leq 1$, whereas subscripts A and B represent two different isotropic

materials. A value of $p \geq 3$ is high enough for compelling ρ_e^p to tend either to 0 or 1. Accordingly, the effective properties at each element $\Omega^{(e)} \in \Omega_{\text{dev}}$ are defined by $\rho_e \equiv P_e$ as the only design variable ($M = 1$), determining which of the two materials A or B is at the finite element $\Omega^{(e)}$.

2.4. Sensitivity analysis

The efficient solution of the optimization problem (13), requires the analytical computation of the derivatives of the objective function f with respect to the design variables $P_i \equiv \rho_i$, $i = 1, 2, \ldots, N$. For computational efficiency, these derivatives can be computed using the adjoint method. For this purpose, the objective function is rewritten as [57–60]:

$$f(\mathbf{P}) = f(\mathbf{P}) - \boldsymbol{\xi}^T (\mathbf{K}\mathbf{T} - \mathbf{Q}) - \boldsymbol{\lambda}^T (\mathbf{K}^{\text{m}}\mathbf{U} - \mathbf{F}), \tag{14}$$

where the additional terms are null by virtue of the FEM-based equilibrium and heat conduction equations (5) and (8), respectively. The differentiation of (14) with respect to P_i yields

$$\frac{\mathrm{d}f}{\mathrm{d}P_i} = \left.\frac{\partial f}{\partial P_i}\right|_{\mathbf{U}=\text{const}} + \frac{\partial f}{\partial \mathbf{U}}\frac{\mathrm{d}\mathbf{U}}{\mathrm{d}P_i} - \boldsymbol{\xi}^T \left(\frac{\partial \mathbf{K}}{\partial P_i}\mathbf{T} + \mathbf{K}\frac{\mathrm{d}\mathbf{T}}{\mathrm{d}P_i} + \hat{\mathbf{K}}\frac{\mathrm{d}\mathbf{T}}{\mathrm{d}P_i}\right) - \boldsymbol{\lambda}^T \left(\frac{\partial \mathbf{K}^{\text{m}}}{\partial P_i}\mathbf{U} + \mathbf{K}^{\text{m}}\frac{\mathrm{d}\mathbf{U}}{\mathrm{d}P_i} + \hat{\mathbf{K}}^{\text{m}}\frac{\mathrm{d}\mathbf{T}}{\mathrm{d}P_i} + \frac{\partial \mathbf{F}^{\text{Th}}}{\partial P_i} + \frac{\partial \mathbf{F}^{\text{Th}}}{\partial \mathbf{T}}\frac{\mathrm{d}\mathbf{T}}{\mathrm{d}P_i}\right), \tag{15}$$

where $\hat{\mathbf{K}}$ and $\hat{\mathbf{K}}^{\text{m}}$ are the matrices with components $\hat{K}_{jk} = (\partial K_{jl}/\partial T_k)T_l$ and $\hat{K}^{\text{m}}_{jk} = (\partial K^{\text{m}}_{jl}/\partial T_k)U_l$, respectively. The matrix $\hat{\mathbf{K}}$ is non null only if thermal conductivity depends on temperature, and also $\hat{\mathbf{K}}^{\text{m}}$ is non null only if the elastic moduli depends on temperature. The terms in (15) can be rearranged as follows:

$$\frac{\mathrm{d}f}{\mathrm{d}P_i} = \left.\frac{\partial f}{\partial P_i}\right|_{\mathbf{U}=\text{const}} + \left(\frac{\partial f}{\partial \mathbf{U}} - \boldsymbol{\lambda}^T\mathbf{K}^{\text{m}}\right)\frac{\mathrm{d}\mathbf{U}}{\mathrm{d}P_i} - \left[\boldsymbol{\lambda}^T\left(\frac{\partial \mathbf{F}^{\text{Th}}}{\partial \mathbf{T}} + \hat{\mathbf{K}}^{\text{m}}\right) + \boldsymbol{\xi}^T\left(\mathbf{K} + \hat{\mathbf{K}}\right)\right]\frac{\mathrm{d}\mathbf{T}}{\mathrm{d}P_i} - \boldsymbol{\lambda}^T\left(\frac{\partial \mathbf{K}^{\text{m}}}{\partial P_i}\mathbf{U} + \frac{\partial \mathbf{F}^{\text{Th}}}{\partial P_i}\right) - \boldsymbol{\xi}^T\frac{\partial \mathbf{K}}{\partial P_i}\mathbf{T}. \tag{16}$$

In order to avoid the expensive computation of $\mathrm{d}\mathbf{T}/\mathrm{d}P_i$ and $\mathrm{d}\mathbf{U}/\mathrm{d}P_i$, the adjoint vectors $\boldsymbol{\lambda}$ and $\boldsymbol{\xi}$ are determined such that:

$$\mathbf{K}^{\text{m}}\boldsymbol{\lambda} = \frac{\partial f}{\partial \mathbf{U}}^T, \tag{17}$$

and

$$\left(\mathbf{K} + \hat{\mathbf{K}}\right)^T \boldsymbol{\xi} = -\left(\frac{\partial \mathbf{F}^{\text{Th}}}{\partial \mathbf{T}} + \hat{\mathbf{K}}^{\text{m}}\right)^T \boldsymbol{\lambda}. \tag{18}$$

Introducing in Eq. (16) the adjoint vectors $\boldsymbol{\lambda}$ and $\boldsymbol{\xi}$ obtained from the solution of (17) and (18), allows the computation of $\mathrm{d}f/\mathrm{d}P_i$ according to:

$$\frac{\mathrm{d}f}{\mathrm{d}P_i} = \left.\frac{\partial f}{\partial P_i}\right|_{\mathbf{U}=\text{const}} - \boldsymbol{\lambda}^T\left(\frac{\partial \mathbf{K}^{\text{m}}}{\partial P_i}\mathbf{U} + \frac{\partial \mathbf{F}^{\text{Th}}}{\partial P_i}\right) - \boldsymbol{\xi}^T\frac{\partial \mathbf{K}}{\partial P_i}\mathbf{T}. \tag{19}$$

It is worth noting that the current objective function (12) does not explicitly depend on $\mathbf{P}$, but only implicitly via $\mathbf{u}(\mathbf{x}^{(h)}, \mathbf{P})$, whereby $\partial f/\partial P_i|_{\mathbf{U}=\text{const}} = 0$.

Similar analyses were performed for the design of functionally graded materials [58], compliant actuators [59] and composites with rectangular inclusions [54], and also in topology optimization thermo-mechanical problems with stress constraints [60]. However, unlike the current study, the work mentioned above have been conducted without considering the dependence of material properties on temperature. Actually, the current sensitivity analysis can be seen as a particular case of the complete formulation developed by Michaleris et al. [57] that includes, besides thermo-dependent material properties, nonlinear and transient effects.

3. Design of an elastostatic cloaking device subjected to thermal loads

As an applied example, the current topology optimization-based procedure will be used in the design of a thermo-mechanical cloaking metadevice.

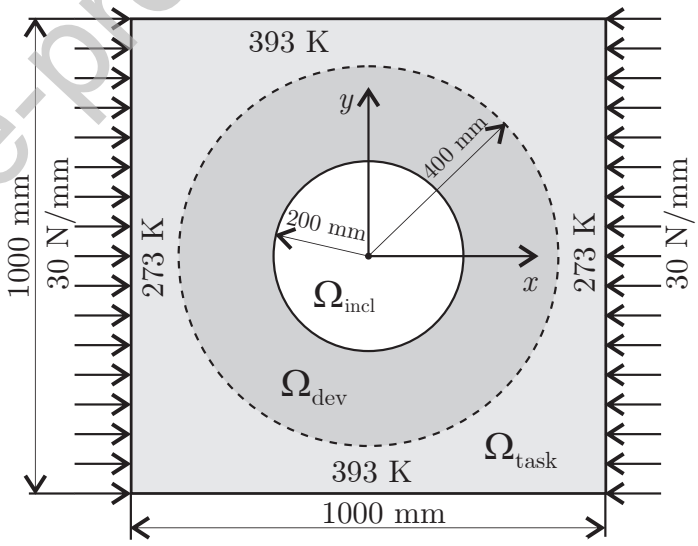

Figure 2: Domain $\Omega = \Omega_{\text{dev}} \cup \Omega_{\text{incl}} \cup \Omega_{\text{task}}$ and boundary conditions of the thermo-mechanical problem.

Let Ω be a full square plate made of nylon (see Table 1 for thermal and mechanical properties) under plane strain conditions, free of internal heat sources and body forces, and subjected to the thermal and mechanical boundary conditions depicted in Fig. 2. Also, let $\mathbf{u}_0$ be the displacement fields in Ω under such conditions. After making a circular hole Ω_{incl} at the center of the plate without altering the boundary conditions mentioned above, the displacements field in Ω is significantly affected. For cloaking purposes, a metadevice occupying the annular region around the hole (Ω_{dev}) will be designed in order to allow the displacement field $\mathbf{u}$ outside the device (Ω_{task}) be affected to a minimum extent. To this end, the optimization problem (13) is solved in order to find $\mathbf{P}$ (the material distribution in Ω_{dev}) such

that the corresponding displacements $\mathbf{u}(\mathbf{x}^{(h)}, \mathbf{P})$ matches – up to a minimum error– the displacements $\mathbf{u}_0(\mathbf{x}^{(h)})$ in the plate before making the hole, at the nodes $\mathbf{x}^{(h)}$ of the finite elements whose centers lie in the region Ω_{task} of the plate outside the device. Such a device will be designed using aluminum (material A) and polyethylene (material B), whose properties are reported in Table 1. The Young's modulus of all the materials are temperature-dependent functions, obtained from a nonlinear regression of the data reported in references [61–63]. It should be noted that the single dependence of the Young's modulus $E(T)$ on temperature introduces variations in both the elastic moduli $\mathbf{C}$ and stress increment per unit temperature $\mathbf{d}$ isotropic tensors, since:

$$\mathbf{C}(T) = \frac{E(T)}{(1+\nu)}\mathbf{I}^{(4)} + \frac{E(T)\nu}{(1+\nu)(1-21\nu)}\mathbf{I}^{(2)} \otimes \mathbf{I}^{(2)},$$

and

$$\mathbf{d}(T) = -\mathbf{C}(T) : \mathbf{I}^{(2)}\alpha,$$

where $\mathbf{I}^{(2)}$ is the second order identity tensor with components $I^{(2)}_{ij} = \delta_{ij}$, whereas $\mathbf{I}^{(4)}$ is the fourth order symmetric identity tensor with components $I^{(4)}_{ijkl} = (\delta_{ik}\delta_{jl} + \delta_{il}\delta_{jk})/2$. The remaining material properties (k, α, ν) are kept constant, since they do no exhibit significant variations within the temperature range inherent to the thermal boundary conditions depicted in Fig. 2. However, it is worth mentioning that the current methodology allows the possibility of introducing the temperature dependence of any property without further complications.

Table 1: Thermal and mechanical properties of nylon, aluminum and polyethylene

Property	**Material**		
	Nylon	Aluminium	Polyethylene
Thermal conductivity [W(mK)$^{-1}$]	0.31	$k_A = 205$	$k_B = 0.46$
Young's modulus [GPa]	$2.33[1.21 - (1 + e^{-0.14\,T(\text{K})+48.5})^{-1}]$	$E_A = -0.04\,T(\text{K}) + 80$	$E_B = 136.16\,e^{-0.016\,T(\text{K})}$
Poisson ratio	0.4	$\nu_A = 0.33$	$\nu_B = 0.46$
Thermal expansion coefficient [K^{-1}]	8×10^{-5}	$\alpha_A = 2.3 \times 10^{-5}$	$\alpha_B = 15 \times 10^{-5}$

3.1. Solution procedure of the optimization problem

Given the symmetry of the domain and thermo-mechanical boundary conditions depicted in Fig. 2, the FEM-based solution of the governing equations will be performed only over the upper right quadrant of Ω by using an uniform mesh of $200 \times 200 = 40000$ bilinear finite elements. The thermo-mechanical problem over the plate with the hole is solved with a mesh of 35053 finite elements, which is obtained after discarding the elements whose centers lie in Ω_{incl}. The artificial density $\rho_e \equiv P_e$ is considered to vary element-wise in Ω_{dev}, which is occupied by 15086 elements. Accordingly, this is a large scale non-linear optimization problem of 15086 design variables subjected to the box constraint $0 \leq P_e \leq 1$. As stated so far, the elastostatic cloaking device will be designed by solving the optimization problem (13), with (12) as the objective function to be minimized. The cloaking task is defined by setting $\bar{\mathbf{u}} = \mathbf{u}_0$ at the nodes $\mathbf{x}^{(h)}$ of those elements whose centers lie in Ω_{task}.

Finally, such a non-linear large-scale constrained optimization problem is solved using the method of moving asymptotes (MMA) [64]. The checkerboard-type instabilities that usually affect this kind of materials distribution problems [33], will be overcome by using the density filtering technique proposed by Bruns and Tortorelli [65]. Such a strategy has already been proven to be well suited for the design of thermal [4, 5, 10, 11], mechanical [15] and thermo-mechanical [16] metadevices. Additionally, Heaviside filtering [66, 67] is implemented in order to reduce the "gray" zones (those elements where $0 < P_e < 1$, i.e. the material is neither aluminum or polyethylene, but an unlikely feasible material with intermediate properties). The combination of both filtering strategies leads to the definition of a filtered artificial density

$$\tilde{P}_e = 1 - \mathrm{e}^{-\beta\bar{P}_e} + \bar{P}_e\mathrm{e}^{-\beta} \equiv \tilde{H}(\bar{P}_e, \beta), \tag{20}$$

with

$$\bar{P}_e = \frac{\sum_{i=1}^{N}\langle r - \Delta_{ei}\rangle P_i}{\sum_{i=1}^{N}\langle r - \Delta_{ei}\rangle}. \tag{21}$$

The above equation defines the density filter [65], being r the filter radius (adopted in this work as 7 times the finite element size), Δ_{ei} the distance between the centers of the elements $\Omega^{(e)}$ and $\Omega^{(i)}$, and $\langle x\rangle = xH(x)$ the ramp function with $H(x)$ denoting the Heaviside step function ($H(x) = 0$ for $x < 0$, $H(0) = 1/2$ and $H(x) = 1$ for $x > 0$). The equation (20) defines the Heaviside projection filtering [68], being $\tilde{H}(x, \beta)$ a regularization of $H(x)$, and β a parameter controlling the curvature of $\tilde{H}$ such that $\tilde{H}(x, 0) \equiv x$ (i.e., there is no filtering) and $\tilde{H}(x, \infty) = H(x)$.

The filtered density $\tilde{P}_e$ is also called "physical" density, since it determines the material properties at the finite element $\Omega^{(e)}$. Consequently, the objective function becomes $\tilde{f}(\mathbf{P}) \equiv f(\tilde{\mathbf{P}})$, but $\mathbf{P}$ remains as design variable. Accordingly, the optimization problem (15) is replaced by

$$\min_{\mathbf{P}\in\mathcal{D}} \tilde{f}(\mathbf{P}) \quad \text{subjected to } 0 \leq P_i \leq 1 \qquad i = 1, 2, \ldots, N, . \tag{22}$$

Filtering has to be accounted within the sensitivity analysis. Since equation (19) now actually defines $\mathrm{d}\tilde{f}/\mathrm{d}\tilde{P}_i$ instead of $\mathrm{d}f/\mathrm{d}P_i$, the derivative of the new objective function with respect to the design variable P_i must be computed using the chain rule:

$$\frac{\mathrm{d}\tilde{f}}{\mathrm{d}P_i} = \frac{\mathrm{d}\tilde{f}}{\mathrm{d}\tilde{P}_j}\frac{\mathrm{d}\tilde{P}_j}{\mathrm{d}\bar{P}_k}\frac{\mathrm{d}\bar{P}_k}{\mathrm{d}P_i},$$

where $\mathrm{d}\tilde{P}_j/\mathrm{d}\bar{P}_k$ and $\mathrm{d}\bar{P}_k/\mathrm{d}P_i$ can be easily derived from equations (20) and (21), respectively.

To obtain the final design, successive optimization problems are solved by gradually increasing β via the continuation method proposed by Andreassen et al. [67], in order to achieve stable convergence and ensuring differentiability in the course of the optimization procedure[66, 67]. This is schematized in the following flowchart in pseudo code:

(1) Initialization: set $s = 0$ and $\mathbf{P}_0 = [0.5,\, 0.5,\, \ldots,\, 0.5]$.

(2) Continuation: set $\beta = 2^s$, $i = 0$ and $\mathbf{P}^{(i)} = \mathbf{P}_0$.

  (a) Thermal FEM: $\tilde{\mathbf{P}} \rightarrow T(\mathbf{x}, \tilde{\mathbf{P}})$

  (b) Mechanical FEM: $(T, \tilde{\mathbf{P}}) \rightarrow \mathbf{u}(\mathbf{x}, \tilde{\mathbf{P}})$

  (c) Objective function: $\mathbf{u}(\mathbf{x}, \tilde{\mathbf{P}}) \rightarrow f(\tilde{\mathbf{P}})$

  (d) Sensitivity: $(\mathbf{P}^{(i)}, \tilde{\mathbf{P}}, \mathbf{u}, T, \ldots) \rightarrow \frac{\partial f}{\partial \tilde{\mathbf{P}}}$

  (e) Update: $\left(\mathbf{P}^{(i)}, \frac{\partial f}{\partial \tilde{\mathbf{P}}}\right) \rightarrow \mathbf{P}^{(i+1)}$

  (f) Stop criterion:

  - If $i < i_{\max}$ and $\|\mathbf{P}^{(i+1)} - \mathbf{P}^{(i)}\|_\infty > \epsilon$, $i \leftarrow i + 1$, go to (a).
  - Otherwise:
    - If $\beta < \beta_{\max}$, set $s \leftarrow s + 1$ and $\mathbf{P}_0 = \mathbf{P}^{(i+1)}$, then go to (2).
    - Otherwise, go to (3).

(3) Thresholding: $(\tilde{\mathbf{P}}, w^*) \rightarrow \tilde{\mathbf{P}}^{\mathrm{thr}}$.

In the above procedure, $\mathbf{P}_0$ is the initial guess, which is first arbitrarily adopted and then updated after each continuation step s. The optimization solver at each continuation step s stops at the iteration $i_{\max} = 300$ or when the change in variables is less than $\epsilon = 0.01$. The curvature of the Heaviside approximation is increased until $\beta_{\max} = 128$, since greater β seriously deteriorate the convergence of the optimization problem. Although the gray zones are considerably reduced after the successive optimization steps, there is still need of a final filtering (the so-called thresholding) to obtain a fully binary design $\tilde{\mathbf{P}}^{\mathrm{thr}}$ with w^* as the threshold for ρ_e^p. The thresholding strategy to be implemented in this work has been proposed by Fachinotti et al.[4, 15], and its implementation will be explained later.

4. Results

The FEM-based solutions for the displacement and temperature fields in the full nylon plate are depicted in Fig. 3 (a)-(c), whereas those in the holed nylon plate are shown in Fig. 3 (d)-(f). After making the hole in the nylon plate, a new displacements field $\mathbf{u}^{\mathrm{hol}}$ is achieved. Such displacements differs considerably from the field $\mathbf{u}_0$ corresponding to the full nylon plate, giving rise to an error $f^{\mathrm{hol}} = 1.203$ in the fulfillment of the cloaking task. The material distribution achieved by solving successive optimization problems (22) via the continuation procedure described in the previous section, is shown in Fig. 4 (a). The displacements and temperature fields achieved when a cloaking device with such a material distribution occupies the annular region bounded by the dashed lines, are depicted in Fig. 3 (g)-(i). Using such a device allows the error in the fulfillment of the cloaking task to be minimized up to a value of $f^{\mathrm{opt}} = 0.01284 = 0.0107 f^{\mathrm{hol}}$, which represents a 98.93% reduction compared to the error f^{hol} corresponding to the holed plate without the device. Even after Heaviside filtering, the optimal solution depicted in Fig. 4 (a) still exhibits gray zones. Such a feature precludes the manufacture of the so-designed thermo-mechanical metadevice, which is a main concern in this work.

In order to suppress the gray zones, recourse can be made to a thresholding strategy proposed in previous work related to the design of both thermal[4] and mechanical[15] easy-to-make metadevices: the material at the element $\Omega^{(e)} \in \Omega_{\mathrm{dev}}$ is aluminum if $\tilde{P}_e^{\mathrm{thr}} = 1$ and polyethylene if $\tilde{P}_e^{\mathrm{thr}} = 0$, with

$$\tilde{P}_e^{\mathrm{thr}} = H(\tilde{P}_e^p - w^*),$$

where w^* is the threshold. In classical topology optimization, w^* is frequently determined in order to fulfill volume constraints [69], although it is frequently conceived as a user-defined parameter [70–75]. In problems without volume constraint like the current one, Fachinotti et al. [4, 15] proposed to determine w^* such that the performance of the metadevice –that is no longer optimal after thresholding– be affected to a minimum extent. In this sense, the thresholding procedure is conceived to find $w^* \in (0, 1)$ such that $f^{\mathrm{thr}} = f(\tilde{\mathbf{P}}^{\mathrm{thr}})$ reaches its minimum. The $f^{\mathrm{thr}}/f^{\mathrm{opt}}$ ratio for different values of w^* is plotted in Fig. 5, which exhibits a minimum at $w^* = 0.12$ where $f^{\mathrm{thr}} = 0.01454 = 1.1324\, f^{\mathrm{opt}} = 0.0120\, f^{\mathrm{hol}}$. Accordingly, using the corresponding discrete device shown in 4 (b) offering the best deal between performance and manufacturability, has allowed a 98.79% reduction compared to the error f^{hol} without the device. The corresponding displacement field $\mathbf{u}^{\mathrm{thr}}$ is depicted in Fig. 3 (j)-(k), whereas the temperature field is shown in Fig. 3 (l). So, losing only 0.14% of the initial displacements field recovery (that of the full nylon plate $\mathbf{u}_0$) in Ω_{task} after the thresholding procedure has allowed the achievement of such a device of feasible manufacture.

The distribution of local relative error $\varepsilon^{\mathrm{hol}} = \|\mathbf{u}^{\mathrm{hol}} - \mathbf{u}_0\|/\|\mathbf{u}_0\|$ for the holed homogeneous plate in the region Ω_{task} –where the cloaking task was prescribed– is depicted in Fig. 6 (a), whereas the distribution of local relative error $\varepsilon^{\mathrm{thr}} = \|\mathbf{u}^{\mathrm{thr}} - \mathbf{u}_0\|/\|\mathbf{u}_0\|$ achieved in the same region when including the thresholded (feasible) cloaking device in Ω_{dev} is depicted in Fig. 6 (b). The good performance of such cloaking device can actually be demonstrated by comparing Fig. 6 (a) and Fig. 6 (b): the maximum $\varepsilon^{\mathrm{thr}}$ is 7.4%, which is less than a half of the minimum $\varepsilon^{\mathrm{hol}}$. These results are also consistent with the deformed contours depicted in Fig. 7, where the displacement are magnified by a factor of 5 for better visualization.

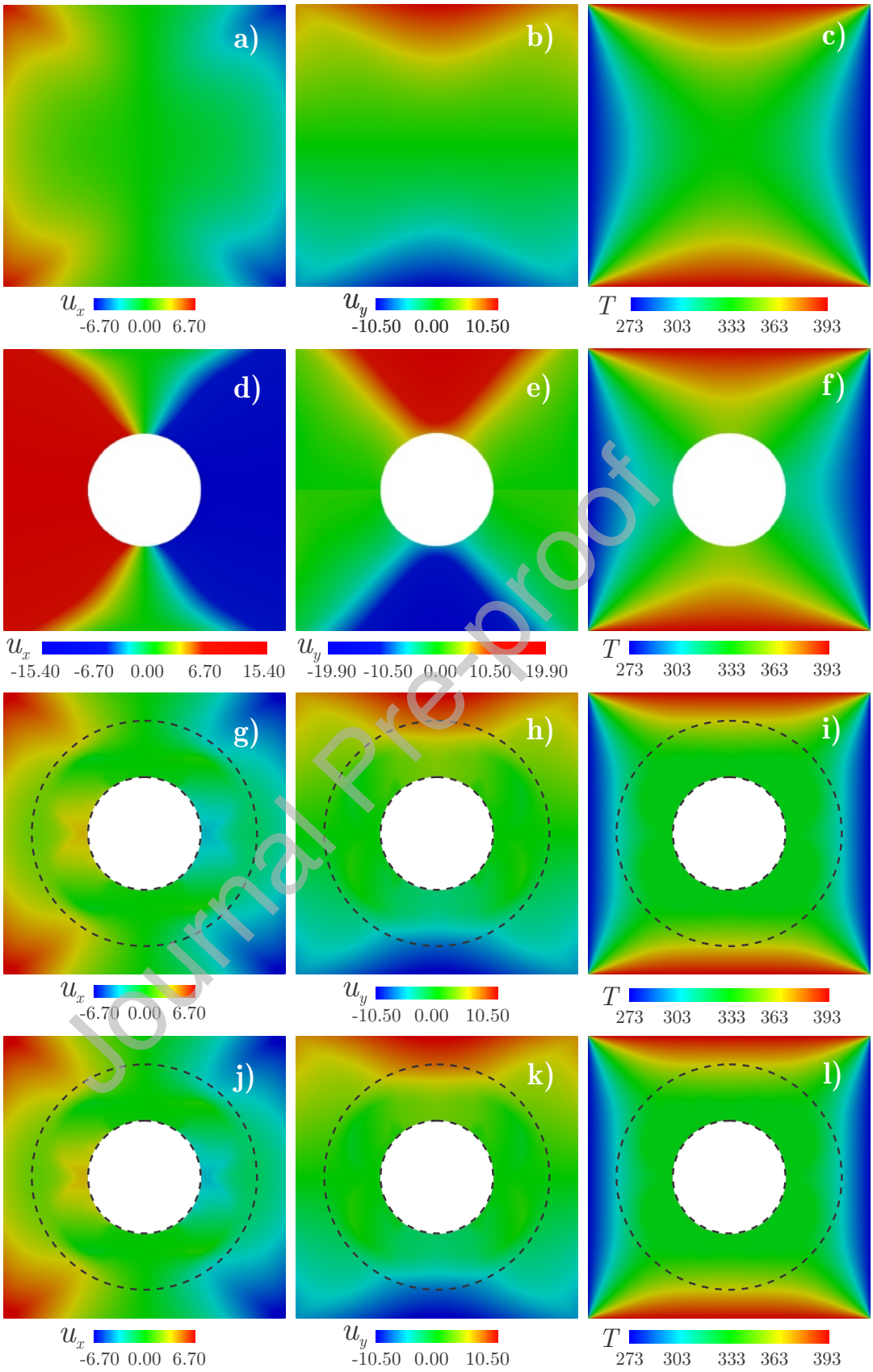

Figure 3: Displacements u_x (a) and u_y (b) and temperature T (c) distributions in the homogeneous plate without hole, the holed homogeneous plate (d-f), the plate with the optimal cloaking device (g-i) and the plate with the fully discrete device (j-l). Displacements and temperature distributions are given in millimeters and Kelvin, respectively.

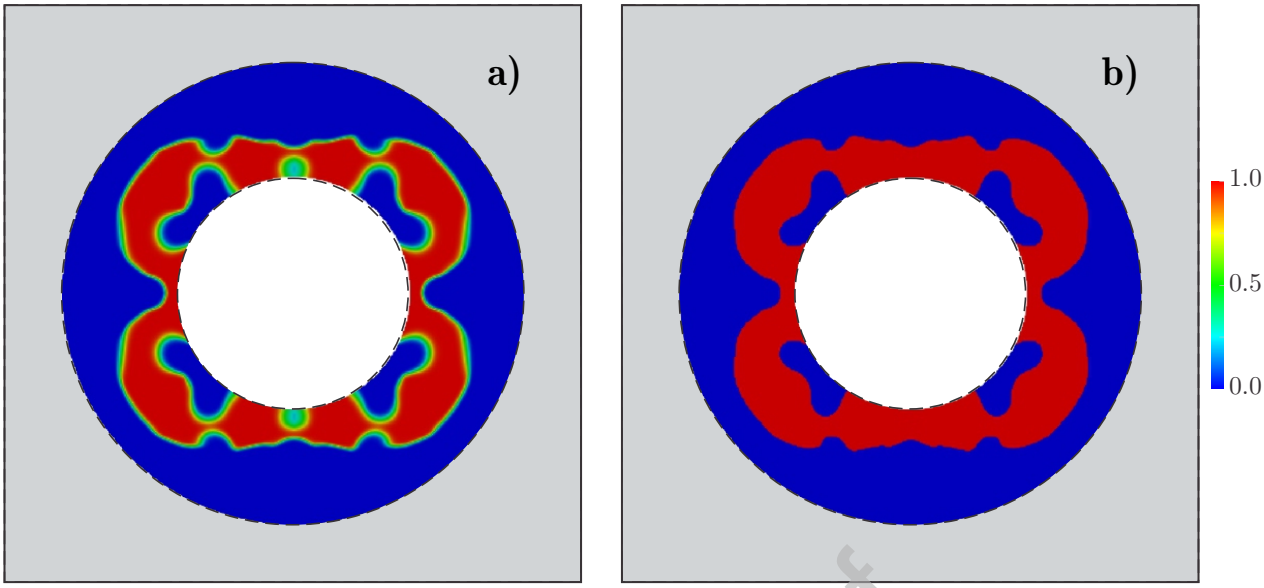

Figure 4: Distribution of aluminum (red) and polyethylene (blue) in the metadevice designed by solving the topology optimization problem. a) Optimal continuous material distribution with gray zones, and b) best discrete material distribution achieved after eliminating the gray zones by thresholding.

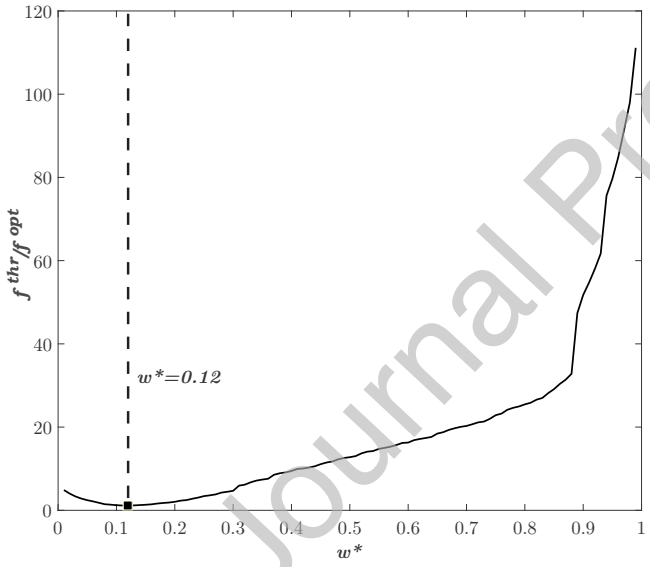

Figure 5: Error in the cloaking task accomplishment by the fully discrete metadevice as a function of the threshold value w^*.

Such deformed contours involve the points lying on the plate boundaries and also on the diagonal lines throughout it, and the deformed contours of the hole and the metadevice are represented by the dotted lines. This figure depicts the marked differences between the deformed shape of the full plate (black) and the holed plate (red), and also the noteworthy overlapping of the contours corresponding to the holed plate with the metadevice (blue) and the full plate (black) in Ω_{task}. Given the significant reduction of the errors with respect to the target displacements field $\mathbf{u}_0$ after introducing the metadevice, the deformed contours corresponding to the full plate and the holed plate with the metadevice are virtually indistinguishable each other in Ω_{task}. These contours also depict how the device works: it is conceived to deform appropriately in order to perform the cloaking task only in Ω_{task}, whereby there is no coincidence of the black and blue contours in the region occupied by such a device (enclosed by the blue dotted lines).

5. Discussion

The results reported in the previous section demonstrate the potential of the current topology optimization-based approach to design thermo-mechanical metadevices, providing a simple and feasible manufacture design consisting of two macroscopically distinguishable isotropic materials. The background material (nylon) has intermediate Young's modulus regarding the metadevice constituents (aluminum and polyethylene), which has already been proven to guarantee an efficient design of metadevices for mechanical cloaking [15]. The background material has also intermediate thermal expansion compared to aluminum and polyethylene, which is actually crucial in the design of thermo-mechanical cloaking devices [16].

As shown in the previous section, the performance of the easy-to-make thresholded cloaking device shown in Fig. 4 (b) is highly satisfactory. A richer design set $\mathcal{D}$ can lead to a metadevice exhibiting even better performance, but that would also be significantly harder to manufacture. For instance, it is possible to design the cloaking device using the same candidate materials, but arranged in laminates of variable relative thickness and orientation.

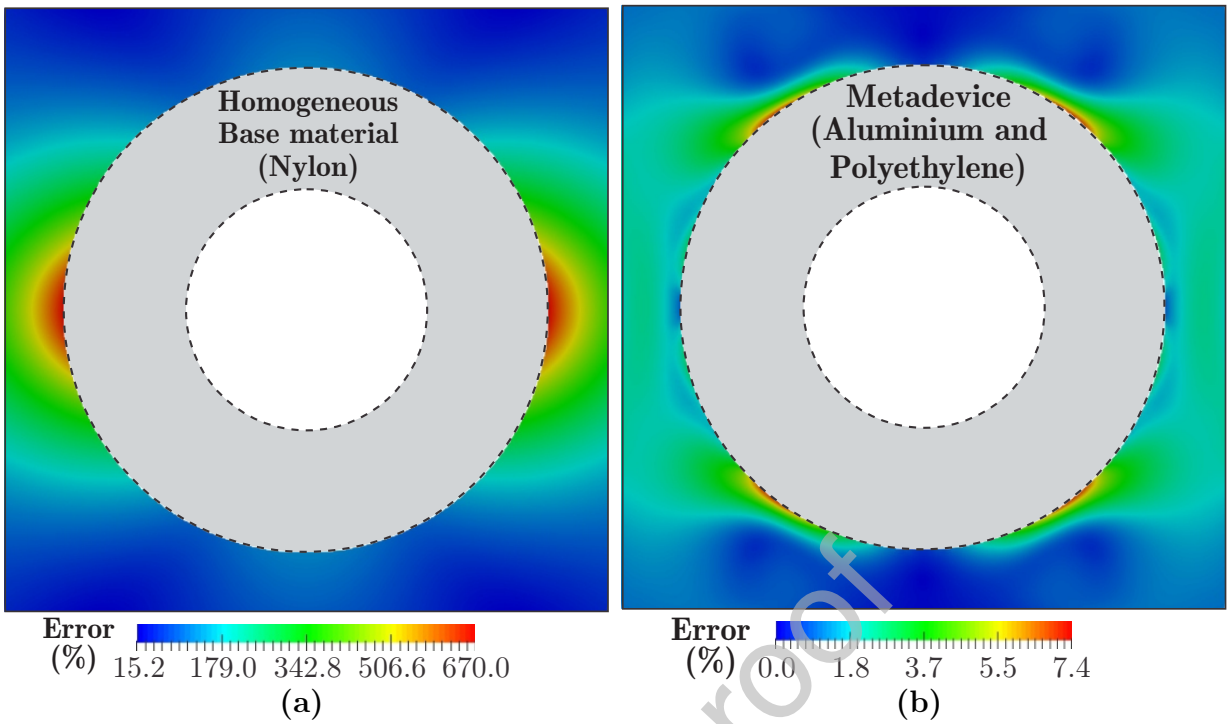

Figure 6: Distribution of local relative error in the cloaking task achievement: (a) Holed homogeneous plate, and (b) Holed plate with the thresholded metadevice.

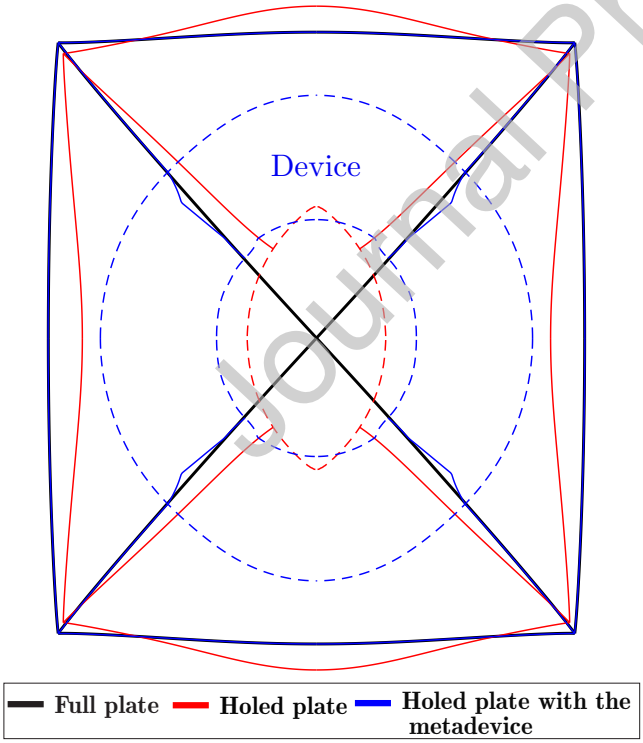

Figure 7: Deformed contours of the internal and external boundaries together to the diagonal lines for the full plate (black), the holed plate (red), and the holed plate with the metadevice (blue).

Such laminates behave as an orthotropic metamaterial, whose properties under plane strain conditions are given in Table 2 [16]. In this case, two design variables are needed to characterize the unit cell at each finite element $\Omega^{(e)}$: the orientation θ_e of the laminate and the relative thickness t_e of the aluminum layer. The relative thickness of the polyethylene layer is simply $1-t_e$, whereby it is not a design variable. So, the metamaterial distribution is determined by solving the problem

$$\min_{\mathbf{P}\in\mathbb{R}^{2N}} f(\bar{\mathbf{P}}) \quad \text{subjected to } 0 \leq P_{2i-1} \leq 1 \text{ and } 0 \leq P_{2i} \leq \pi, \quad i = 1, 2, \ldots, N, \quad (23)$$

where $\mathbf{P}$ is the set of design variables $P_{2i-1} = t_i$ and $P_{2i} = \theta_i$, whereas $\bar{\mathbf{P}}$ is that of density-filtered variables $\bar{P}_{2i-1} = \bar{t}_i$ and $\bar{P}_{2i} = \bar{\theta}_i$ defined in terms of their respective design variables by equation (21). The effective properties within such a richer design set support intermediate values between those of aluminum and polyethylene, whereby gray zones are not penalized and there is no Heaviside filtering.

Note that problem (23) has twice as many design variables as (22), becoming considerably more expensive to solve. The solution of (23), once density-filtered, gives rise to the metamaterial distribution shown in Fig. 8. The colormap indicates the relative thickness of the aluminum layers, whereas the black segments represent the laminates orientation.

Table 2: Effective thermal and mechanical properties of a laminate consisting in two layers of materials A and B with respective relative thicknesses $t_A \equiv t_e$ and $t_B = 1 - t_e$, referred to the local Cartesian frame $\lambda\tau$ (λ in the laminate direction, and τ across the laminate).

Thermal conductivity	$k_{\lambda\lambda} = t_\mathrm{A} k_\mathrm{A} + t_\mathrm{B} k_\mathrm{B}$
	$k_{\tau\tau} = k_\mathrm{A} k_\mathrm{B} (t_\mathrm{A} k_\mathrm{B} + t_\mathrm{B} k_\mathrm{A})^{-1}$
Elastic moduli	$C_{\lambda\lambda\lambda\lambda} = E_\lambda (1 - \nu_{\lambda\tau}\nu_{\tau\lambda})[1 - \nu_{\lambda z}^2 - 2\nu_{\lambda\tau}\nu_{\tau\lambda}(1 + \nu_{\lambda z})]^{-1}$
	$C_{\tau\tau\tau\tau} = E_\tau (1 - \nu_{\lambda z})(1 - 2\nu_{\lambda\tau}\nu_{\tau\lambda} - \nu_{\lambda z})^{-1}$
	$C_{\lambda\lambda\tau\tau} = E_\tau \nu_{\lambda\tau}(1 - 2\nu_{\lambda\tau}\nu_{\tau\lambda} - \nu_{\lambda z})^{-1}$
	$C_{\lambda\tau\lambda\tau} = G_{\lambda\tau}$
Young's moduli	$E_\lambda = [E_\mathrm{A} t_\mathrm{A} (1 - \nu_\mathrm{A}^2)^{-1} + E_\mathrm{B} t_\mathrm{B} (1 - \nu_\mathrm{B}^2)^{-1}](1 - \nu_{\lambda z}^2)$
	$E_\tau = \big[(1 - 2\nu_\mathrm{A})(1 + \nu_\mathrm{A}) t_\mathrm{A} (E_\mathrm{A}(1 - \nu_\mathrm{A}))^{-1} \ldots$
	$+ (1 - 2\nu_\mathrm{B})(1 + \nu_\mathrm{B}) t_\mathrm{B} (E_\mathrm{B}(1 - \nu_\mathrm{B}))^{-1} + 2\nu_{\lambda\tau}^2 (E_\lambda (1 - \nu_{\lambda z}))^{-1}\big]^{-1}$
Poisson ratii	$\nu_{\lambda z} = [E_\mathrm{A} t_\mathrm{A} \nu_\mathrm{A} (1 - \nu_\mathrm{A}^2)^{-1} + E_\mathrm{B} t_\mathrm{B} \nu_\mathrm{B} (1 - \nu_\mathrm{B}^2)^{-1}][E_\mathrm{A} t_\mathrm{A} (1 - \nu_\mathrm{A}^2)^{-1} + E_\mathrm{B} t_\mathrm{B} (1 - \nu_\mathrm{B}^2)^{-1}]^{-1}$
	$\nu_{\lambda\tau} = [\nu_\mathrm{A} t_\mathrm{A} (1 - \nu_\mathrm{A})^{-1} + \nu_\mathrm{B} t_\mathrm{B} (1 - \nu_\mathrm{B})^{-1}](1 - \nu_\lambda z)$
	$\nu_{\tau\lambda} = \nu_{\lambda\tau} E_\tau E_\lambda^{-1}$
Shear modulus	$G_{\lambda\tau} = G_\mathrm{A} G_\mathrm{B} (t_\mathrm{A} G_\mathrm{B} + t_\mathrm{B} G_\mathrm{A})^{-1}$
Thermal expansion	$\alpha_{\lambda\lambda} = [\alpha_\mathrm{A} E_\mathrm{A} t_\mathrm{A} (1 - \nu_\mathrm{A})^{-1} + \alpha_\mathrm{B} E_\mathrm{B} t_\mathrm{B} (1 - \nu_\mathrm{A})^{-1}](1 - \nu_{\lambda z}) E_\lambda^{-1}$
	$\alpha_{\tau\tau} = \alpha_\mathrm{A} t_\mathrm{A} (1 + \nu_\mathrm{A})(1 - \nu_\mathrm{A})^{-1} + \alpha_\mathrm{B} t_\mathrm{B} (1 + \nu_\mathrm{B})(1 - \nu_\mathrm{B})^{-1} - 2\nu_{\lambda\tau}\alpha_{\lambda\lambda}(1 - \nu_{\lambda z})^{-1}$

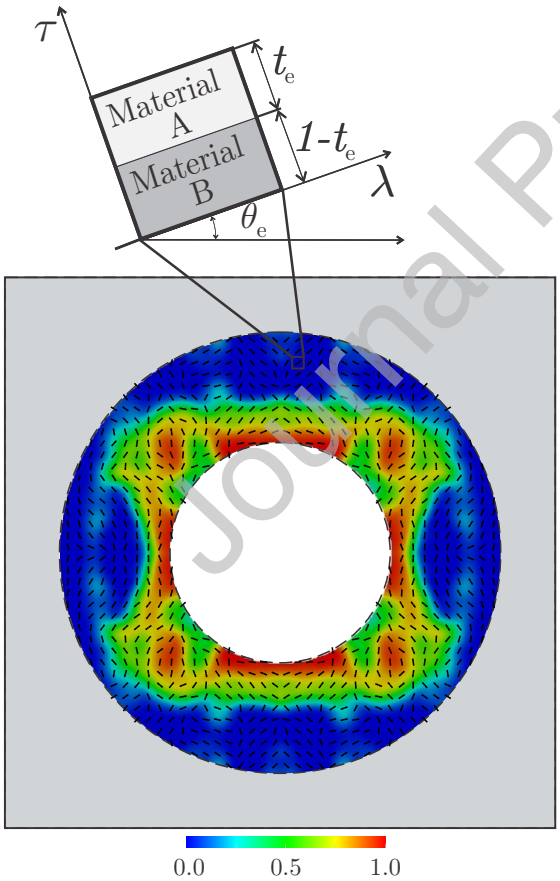

Figure 8: Variable relative thickness of the aluminum layer (colormap) and orientation (black segments) of the optimal heterogeneous metadevice made of laminates of aluminum and polyethylene. On the top, unit cell at a finite element in the metadevice.

Using this completely heterogeneous optimal metadevice allows the error in the fulfillment of the cloaking task to be minimized up to a value of $f^\mathrm{het} = 0.00753 = 0.0063 f^\mathrm{hol}$, which represents a 99.37% reduction compared to the error f^hol corresponding to the holed plate without the device.

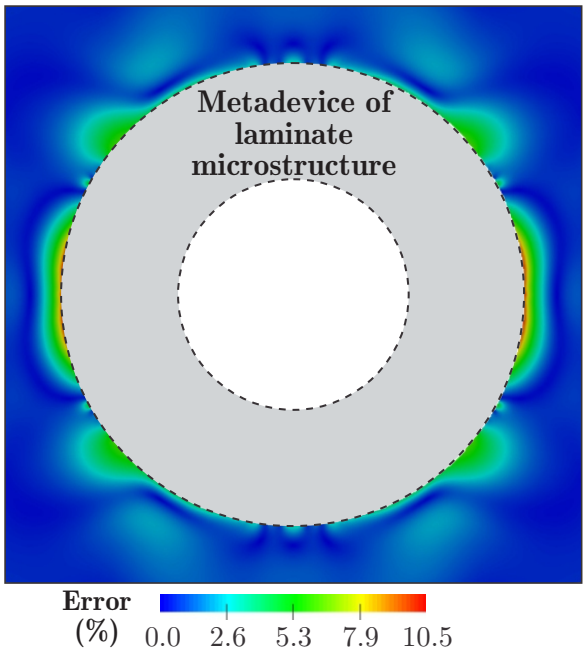

Figure 9: Distribution of local relative error in the cloaking task achievement in the holed plate with the optimal heterogeneous metadevice made of laminates of aluminum and polyethylene.

The distribution of local relative error $\varepsilon^\mathrm{het} = \|\mathbf{u}^\mathrm{het} - \mathbf{u}_0\|/\|\mathbf{u}_0\|$ (being $\mathbf{u}^\mathrm{het}$ the displacement field in presence of

this metadevice) in the region Ω_{task} is depicted in Fig. 9, and exhibits a maximum value $\max \varepsilon^{\text{het}} = 10.5\%$. Compared to the thresholded metadevice (Fig. 4 (b)), the optimal heterogeneous metadevice (Fig. 8) performs the cloaking task globally better ($f^{\text{het}} = 0.5179 f^{\text{thr}}$) but locally worse ($\max \varepsilon^{\text{het}} = 1.4189 \max \varepsilon^{\text{thr}}$). In conclusion, although it is slightly less efficient to globally accomplish the cloaking task, the thresholded metadevice is largely preferred thanks to its feasibility.

5.1. Importance of including temperature-dependent properties

The significance of accounting for the thermal-dependence of material properties in the design of manufacturable thermo-mechanical devices is a feature that – up to the authors' knowledge– is considered for the first time in this work. Such an aspect can actually be demonstrated by solving again the topology optimization thermo-mechanical problem discussed so far, but neglecting the thermal-dependence of Young's modulus of all the involved materials. For such a purpose, the Young's modulus of the materials will be computed at the average value of the temperature range involved in the thermo-mechanical problem ($T = 333$ K). Following the procedure described in Section 3.1. in the framework of this thermo-mechanical problem, the thresholded device depicted in Fig. 10 is obtained. Such a metadevice exhibits noteworthy differences in the material distribution with respect to the thresholded device shown in Fig. 4 (b), which was designed taking due account of the thermal-dependence of Young's moduli.

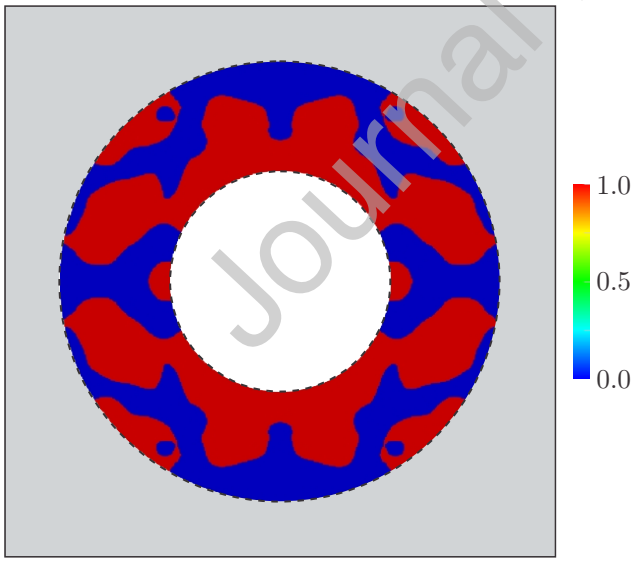

Figure 10: Distribution of aluminum (red) and polyethylene (blue) in the thresholded metadevice obtained after neglecting the thermal-dependence of the Young's modulus of all the involved materials.

Keeping in mind that the displacement field to be recovered is actually that of the full plate made of nylon with thermo-dependent Young's modulus (the field $\mathbf{u}_0$ shown in Fig. 3 (a) and (b)), the error in the cloaking task achievement using the metadevice shown in Fig. 10 is $f^{\text{con}} = 0.392 = 26.9601 f^{\text{thr}}$ (much higher than the error f^{thr} for thresholded metadevice in the Fig. 4 (b)). The poor performance of this device is a consequence of having been conceived to fulfill the cloaking task under conditions such that the properties of all the materials involved can be considered constant, which is not realistic given that the Young's modulus of such materials exhibit actually noteworthy variations in the temperature range of the thermo-mechanical problem addressed in this work. In conclusion, neglecting the thermal-dependence of material properties may seriously deteriorate the performance of the metadevice.

5.2. Versatility of the topology optimization-based approach

To further highlight the versatility of the current topology optimization-based approach for the design of thermo-mechanical metadevices, the design of a different cloaking device will be carried out under the geometric configuration shown in Fig. 11. This problem is identical to that described in Section 4., but introducing changes in the geometry of both the hole Ω_{incl} and the metadevice Ω_{dev}. The geometry of the hole is changed to a rhombus, whereas the metadevice is now a square surrounding the hole. Such modification in the geometry makes more difficult the search for an invariant form of the conservation equations, when using the classical coordinates transformation-based design approaches [7, 23, 25, 26, 28]. However, when the current topology optimization-based approach is used, the design process is identical to that described in Section 3.1.

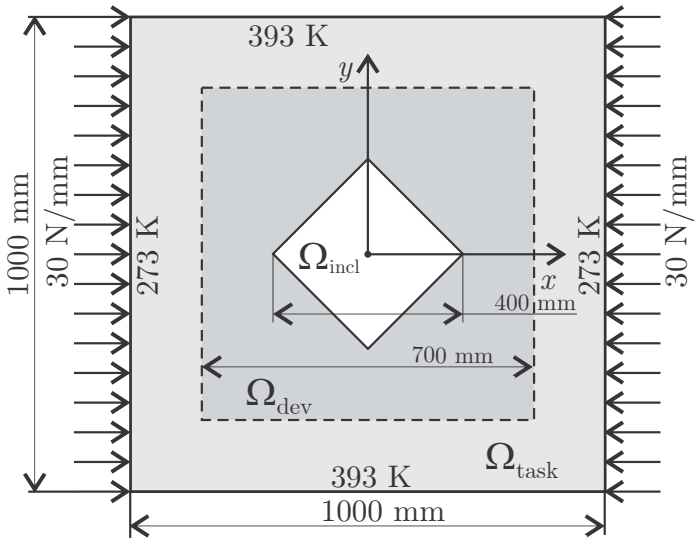

Figure 11: Domain $\Omega = \Omega_{\text{dev}} \cup \Omega_{\text{incl}} \cup \Omega_{\text{task}}$ and boundary conditions of the thermo-mechanical problem with different geometries for both the hole and the cloaking device.

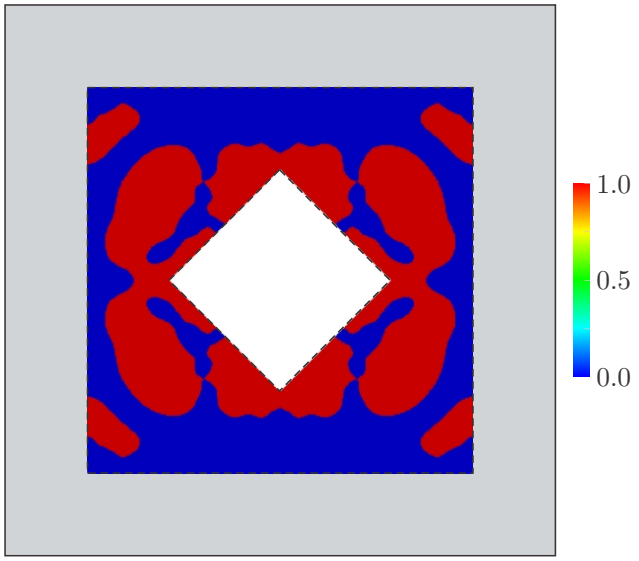

Figure 12: Distribution of aluminum (red) and polyethylene (blue) in the metadevice achieved under the proposed topology optimization-based approach, when considering different geometries for both the hole and the metadevice

After making the rhombic hole in the plate, the changes in the displacements field compared to that of the full plate (the field $\mathbf{u}_0$ shown in Fig. 3 (a) and (b)) give rise to a global error $f^{\diamond \mathrm{hol}} = 0.89$ in the accomplishment of the cloaking task throughout Ω_{task}. The distribution of local relative error $\varepsilon^{\diamond \mathrm{hol}} = \|\mathbf{u}^{\diamond \mathrm{hol}} - \mathbf{u}_0\|/\|\mathbf{u}_0\|$, with $\mathbf{u}^{\diamond \mathrm{hol}}$ denoting the displacement in this holed plate, is depicted in Fig. 13 (a). Such a distribution exhibits maximum value of $\max \varepsilon^{\diamond \mathrm{hol}} = 616\%$.

The fully discrete metadevice shown in Fig. 12 has been obtained by following the same steps detailed in section 3.1., finding a threshold of $w^* = 0.08$ that guarantees the best deal between performance and manufacturability. Using this device reduces the error in the cloaking task up to $f^{\diamond \mathrm{thr}} = 0.0255 = 0.0287 f^{\diamond \mathrm{hol}}$, which represents a 97.13% reduction compared to the error $f^{\diamond \mathrm{hol}}$ corresponding to the holed plate without metadevice. Fig. 13 (b) shows the distribution of local relative error $\varepsilon^{\diamond \mathrm{thr}} = \|\mathbf{u}^{\diamond \mathrm{thr}} - \mathbf{u}_0\|/\|\mathbf{u}_0\|$, with $\mathbf{u}^{\diamond \mathrm{thr}}$ denoting the displacement in this holed plate when including in Ω_{dev} the metadevice depicted in Fig. 12.

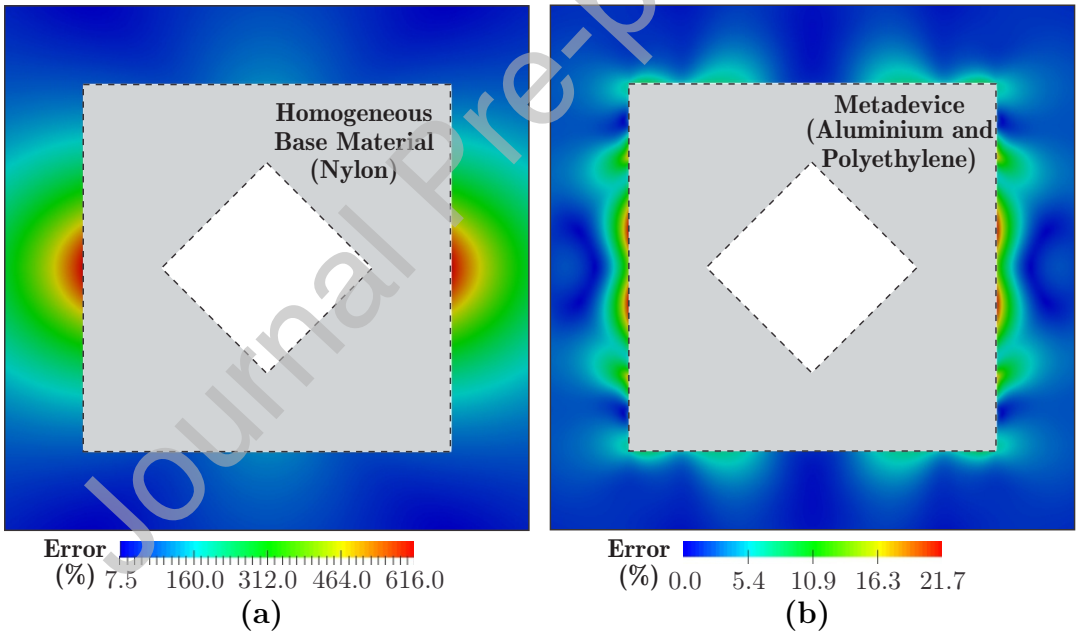

Figure 13: Distribution of local relative error in the cloaking task achievement: (a) Holed homogeneous plate, and (b) Holed plate with the thresholded metadevice.

Note that using this feasible metadevice considerably reduces the maximum local relative error up to $\max \varepsilon^{\diamond \mathrm{thr}} = 21.7\% = 0.0352 \max \varepsilon^{\diamond \mathrm{hol}}$.

Finally, the good performance of this cloaking metadevice is qualitatively appreciated in the deformed contours depicted in Fig. 14 corresponding to the full plate as well as of the holed plate with and without the metadevice, where the displacements are magnified by a factor of 5 for better visualization. Including the metadevice designed in this alternative case, has also given rise to a noteworthy overlapping of the deformed contours in Ω_{task}. Despite the changes introduced in the problem geometry, the cloaking device still works the way it was intended.

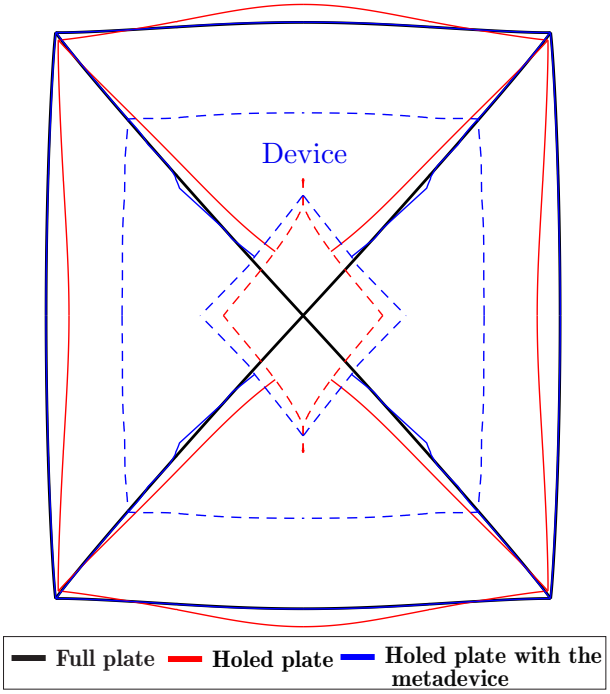

Figure 14: Deformed contours of the internal and external boundaries together to the diagonal lines for the full plate (black), the holed plate (red), and the holed plate with the metadevice (blue).

6. Conclusions

A novel approach has been introduced for the computational design of manufacturable thermo-mechanical metadevices, accounting for the coupling between temperature and displacement fields when both are actually influenced by the material distribution. It consists in the solution of a topology optimization problem where the objective function defines the error in the accomplishment of a displacement-dependent task (cloaking, particularly), and the design variables determine the material distribution. This topology optimization problem is solved using the popular solid isotropic microstructure (or material) with penalization (SIMP) interpolation scheme, where the design variable is an artificial density serving to choose between two candidate materials with contrasting thermal and mechanical properties.

Compared to a previous communication also concerning the design of thermo-mechanical devices considering the coupling and design-dependence of temperature and displacement [16], the current work introduces manufacturability as a crucial contribution. Metadevices are made of only two macroscopically distinguishable standard isotropic materials, being easy-to-make, unlike the previously designed heterogeneous metadevices [16] made of orthotropic laminate-based metamaterials.

The thermo-mechanical response of the device is evaluated using the finite element method, allowing fully arbitrary geometries for the device, the domain where it is embedded and its thermal and mechanical boundary conditions, which largely contributes to the high versatility of the currently proposed approach.

The potentiality and versatility of the proposed topology optimization-based approach are demonstrated via its application to the design of a series of elastostatic cloaking metadevices in regions subjected to thermal and mechanical loads, considering either constant or temperature-dependent material properties and different geometries. All the so-designed cloaking metadevices are easy-to-make, exhibiting also a good performance.

Further, in so doing, it was highlighted the importance of the thermal-dependence of material properties on the thermo-mechanical response of the metadevice, and consequently in its final design.

It was also demonstrated that an unique approach serves for different problems.

Based on the obtained results, the following conclusions can be highlighted: (i) the proposed topology optimization-based approach allows the design of manufacturable and high-performance thermo-mechanical metadevices; (ii) the so-designed metadevices can be easily manufactured using two macroscopically distinguishable isotropic materials with contrasting material properties; (iii) the effect of material distribution on temperature was accounted for, which is unprecedented in the design of manufacturable thermo-mechanical metadevices; (iv) by considering the influence of material distribution on temperature, the thermal-dependence of material properties and the coupling of temperature and displacement fields, the current approach allows solving problems that are unaffordable with the classical coordinates transformation-based approach for the design of metamaterials and metadevices; and (v) the material distribution in the thermo-mechanical metadevice is prescribed, which is a crucial advantage with respect to the approaches (like the transformation-based one) that define inhomogeneous and uncertainly feasible material properties.

Acknowledgements

The authors gratefully acknowledge the financial support from:

- The National Scientific and Technical Research Council (CONICET) of Argentina.
- - The Argentine Agency for Scientific and Technological Promotion (ANPCyT), through the project “Computational Design of Metamaterials” (PICT-2016-2673).
- - The National Littoral University (UNL) at Santa Fe, Argentina, through the project “Metamaterials: Com-

putational Design, Thermal, Mechanical and Acoustic Applications, and Prototyping" (CAI+D 2016 087LI).

- - The National Technological University (UTN) of Argentina, for Grant PID MAUTNFE0007745.

References

[1] Dang Minh Nguyen, Hongyi Xu, Youming Zhang, and Baile Zhang. Active thermal cloak. *Applied Physics Letters*, 107(12):121901, 2015.

[2] Xiangying Shen, Ying Li, Chaoran Jiang, Yushan Ni, and Jiping Huang. Thermal cloak-concentrator. *Applied Physics Letters*, 109(3):031907, 2016.

[3] T.-Z. Yang, Y. Su, W. Xu, and X. D-Yang. Transient thermal camouflage and heat signature control. *Applied Physics Letters*, 109:121905, 2016.

[4] Víctor D. Fachinotti, Ángel A. Ciarbonetti, Ignacio Peralta, and Ignacio Rintoul. Optimization-based design of easy-to-make devices for heat flux manipulation. *International Journal of Thermal Sciences*, 128:38–48, 2018.

[5] Juan C. Álvarez Hostos, Víctor D. Fachinotti, Ignacio Peralta, and Benjamín A. Tourn. Computational design of metadevices for heat flux manipulation considering the transient regime. *Numerical Heat Transfer, Part A: Applications*, pages 1–16, 2019.

[6] Ignacio Peralta, Víctor D. Fachinotti, and Juan C. Álvarez Hostos. A Brief Review on Thermal Metamaterials for Cloaking and Heat Flux Manipulation. *Advanced Engineering Materials*, 22(2):1901034, nov 2019.

[7] Muamer Kadic, Tiemo Bückmann, Robert Schittny, and Martin Wegener. Metamaterials beyond electromagnetism. *Reports on Progress in Physics*, 76(12):126501, 2013.

[8] Ercan M. Dede, Tsuyoshi Nomura, Paul Schmalenberg, and Jae Seung Lee. Heat flux cloaking, focusing, and reversal in ultra-thin composites considering conduction-convection effects. *Applied Physics Letters*, 103(6):063501, 2013.

[9] F. Chen and D. Y. Lei. Experimental Realization of Extreme Heat Flux Concentration with Easy-to-Make Thermal Metamaterials. *Scientific Reports*, 5:11552, 2015.

[10] Ignacio Peralta, Víctor D. Fachinotti, and Ángel A. Ciarbonetti. Optimization-based design of a heat flux concentrator. *Scientific Reports*, 7(1), 2017.

[11] Ignacio Peralta and Víctor D. Fachinotti. Optimization-based design of heat flux manipulation devices with emphasis on fabricability. *Scientific Reports*, 7(6261), 2017.

[12] Krishna P. Vemuri, Fatih M. Cambazoglu, and Prabhakar R. Bandaru. Guiding conductive heat flux through thermal metamaterials. *Applied Physics Letters*, 105(19):193904, 2014.

[13] Tiemo Bückmann, Michael Thiel, Muamer Kadic, Robert Schittny, and Martin Wegener. An elasto-mechanical unfeelability cloak made of pentamode metamaterials. *Nature Communications*, 5(1), 2014.

[14] Tiemo Bückmann, Muamer Kadic, Robert Schittny, and Martin Wegener. Mechanical cloak design by direct lattice transformation. *Proceedings of the National Academy of Sciences*, 112(16):4930–4934, 2015.

[15] Víctor D. Fachinotti, Ignacio Peralta, and Alejandro E. Albanesi. Optimization-based design of an elastostatic cloaking device. *Scientific Reports*, 8(1), 2018.

[16] Juan C. Álvarez Hostos, Víctor D. Fachinotti, and Ignacio Peralta. Metamaterial for elastostatic cloaking under thermal gradients. *Scientific Reports*, 9(1), 2019.

[17] Nicolas Stenger, Manfred Wilhelm, and Martin Wegener. Experiments on Elastic Cloaking in Thin Plates. *Physical Review Letters*, 108(1):014301, 2012.

[18] Muamer Kadic, Tiemo Bückmann, Robert Schittny, and Martin Wegener. Experiments on cloaking in optics, thermodynamics and mechanics. *Philosophical Transactions of the Royal Society A: Mathematical, Physical and Engineering Sciences*, 373(2049):20140357, 2015.

[19] Min Kyung Lee and Yoon Young Kim. Add-on unidirectional elastic metamaterial plate cloak. *Scientific Reports*, 6(1):20731, 2016.

[20] Chunyu Ren and Zhihai Xiang. Camouflage devices with simplified material parameters based on conformal transformation acoustics. *Applied Mathematical Modelling*, 38(15-16):3774–3780, 2014.

[21] Ulf Leonhardt. Optical Conformal Mapping. *Science*, 312:1777–1780, 2006.

[22] John B. Pendry, David Schurig, and David R. Smith. Controlling electromagnetic fields. *Science*, 312(5781):1780–1782, 2006.

[23] Andrew N. Norris and Alexander L. Shuvalov. Elastic cloaking theory. *Wave Motion*, 48:525–538, 2011.

[24] John R. Willis. Variational principles for dynamic problems for inhomogeneous elastic media. *Wave Motion*, 3:1–11, 1981.

[25] Graeme W. Milton, Marc Briane, and John R. Willis. On cloaking for elasticity and physical equations with a transformation invariant form. *New Journal of Physics*, 8, 2006.

[26] Michele Brun, Sébastien Guenneau, and Alexander B. Movchan. Achieving control of in-plane elastic waves. *Applied Physics Letters*, 94(6):061903, 2009.

[27] Muamer Kadic, Tiemo Bückmann, Nicolas Stenger, Michael Thiel, and Martin Wegener. On the practicability of pentamode mechanical metamaterials. *Applied Physics Letters*, 100(19):191901, 2012.

[28] Mohamed Farhat, Sebastien Guenneau, and Stefan Enoch. Ultrabroadband Elastic Cloaking in Thin Plates. *Physical Review Letters*, 103(2), 2009.

[29] Lucas Colabella, Adrián P. Cisilino, Victor Fachinotti, and Piotr Kowalczyk. Multiscale design of elastic solids with biomimetic cancellous bone cellular microstructures. *Structural and Multidisciplinary Optimization*, 60(2):639–661, 2019.

[30] Lucas Colabella, Adrián Cisilino, Victor Fachinotti, Carlos Capiel, and Piotr Kowalczyk. Multiscale design of artificial bones with biomimetic elastic microstructures. *Journal of the Mechanical Behavior of Biomedical Materials*, 108:103748, 2020.

[31] Ole Sigmund and Salvatore Torquato. Composites with extremal thermal expansion coefficients. *Applied Physics Letters*, 69(21):3203–3205, 1996.

[32] O. Sigmund and S. Torquato. Design of materials with extreme thermal expansion using a three-phase topology optimization method. *Journal of the Mechanics and Physics of Solids*, 45(6):1037–1067, 1997.

[33] Martin P. Bendsøe and Ole Sigmund. *Topology optimization. Theory, methods, and applications*. Springer-Verlag, 2003.

[34] Xiaoming Wang, Yulin Mei, and Michael Yu Wang. Level-set method for design of multi-phase elastic and thermoelastic materials. *International Journal of Mechanics and Materials in Design*, 1(3):213–239, 2004.

[35] Akihiro Takezawa, Makoto Kobashi, and Mitsuru Kitamura. Porous composite with negative thermal expansion obtained by photopolymer additive manufacturing. *APL Materials*, 3(7):076103, 2015.

[36] Yu Wang, Zhen Luo, Nong Zhang, and Tao Wu. Topological design for mechanical metamaterials using a multiphase level set method. *Structural and Multidisciplinary Optimization*, 54(4):937–952, 2016.

[37] Yu Wang, Jie Gao, Zhen Luo, Terry Brown, and Nong Zhang. Level-set topology optimization for multimaterial and multifunctional mechanical metamaterials. *Engineering Optimization*, 49(1):22–42, 2016.

[38] Seth Watts and Daniel A. Tortorelli. Optimality of thermal expansion bounds in three dimensions. *Extreme Mechanics Letters*, 12:97–100, 2017.

[39] Ole Sigmund and Kurt Maute. Topology optimization approaches. *Structural and Multidisciplinary Optimization*, 48(6):1031–1055, 2013.

[40] Renato Picelli, Scott Townsend, Christopher Brampton, Julian Norato, and Hyunsun A. Kim. Stress-based shape and topology optimization with the level set method. *Computer Methods in Applied Mechanics and Engineering*, 329:1–23, 2018.

[41] Dixiong Yang, Hongliang Liu, Weisheng Zhang, and Shi Li. Stress-constrained topology optimization based on maximum stress measures. *Computers & Structures*, 198:23–39, 2018.

[42] Alberto Pizzolato, Ashesh Sharma, Kurt Maute, Adriano Sciacovelli, and Vittorio Verda. Topology optimization for heat transfer enhancement in latent heat thermal energy storage. *International Journal of Heat and Mass Transfer*, 113:875–888, 2017.

[43] Suna Yan, Fengwen Wang, and Ole Sigmund. On the non-optimality of tree structures for heat conduction. *International Journal of Heat and Mass Transfer*, 122:660–680, 2018.

[44] Alexandre Molter, Jun Sérgio Ono Fonseca, and Lucas dos Santos Fernandez. Simultaneous topology optimization of structure and piezoelectric actuators distribution. *Applied Mathematical Modelling*, 40(9-10):5576–5588, 2016.

[45] Xianbao Duan, Xinqiang Qin, and Feifei Li. Topology optimization of stokes flow using an implicit coupled level set method. *Applied Mathematical Modelling*, 40(9-10):5431–5441, 2016.

[46] Seung Hyun Jeong, Jong Wook Lee, Gil Ho Yoon, and Dong Hoon Choi. Topology optimization considering the fatigue constraint of variable amplitude load based on the equivalent static load approach. *Applied Mathematical Modelling*, 56:626–647, 2018.

[47] Seung Hyun Jeong, Dong-Hoon Choi, and Gil Ho Yoon. Fatigue and static failure considerations using a topology optimization method. *Applied Mathematical Modelling*, 39(3-4):1137–1162, 2015.

[48] Tong Gao, Pengli Xu, and Weihong Zhang. Topology optimization of thermo-elastic structures with multiple materials under mass constraint. *Computers & Structures*, 173:150–160, 2016.

[49] Evert C. Hooijkamp and Fred van Keulen. Topology optimization for linear thermo-mechanical transient problems: Modal reduction and adjoint sensitivities. *International Journal for Numerical Methods in Engineering*, 113(8):1230–1257, 2017.

[50] Luis Augusto Motta Mello, Ruben Andres Salas, and Emílio Carlos Nelli Silva. On response time reduction of electrothermomechanical MEMS using topology optimization. *Computer Methods in Applied Mechanics and Engineering*, 247-248:93–102, 2012.

[51] S. Narayana and Y. Sato. Heat flux manipulation with engineered thermal materials. *Physical Review Letters*, 108(21):214303, 2012.

[52] Akihiro Takezawa, Shinji Nishiwaki, and Mitsuru Kitamura. Shape and topology optimization based on the phase field method and sensitivity analysis. *Journal of Computational Physics*, 229(7):2697–2718, 2010.

[53] J. Stegmann and E. Lund. Discrete material optimization of general composite shell structures. *Int. J. Numer. Meth. Engng*, 62:20092027, 2005.

[54] Víctor D. Fachinotti, Sebastián Toro, Pablo J. Sánchez, and Alfredo E. Huespe. Sensitivity of the thermomechanical response of elastic structures to microstructural changes. *International Journal of Solids and Structures*, 69-70:45–59, 2015.

[55] Richard Craster, Andre Diatta, Sebastien Guenneau, and Harsha Hutridurga. Some results in near-cloaking for elasticity systems.

[56] R V Kohn, H Shen, M S Vogelius, and M I Weinstein. Cloaking via change of variables in electric impedance tomography. *Inverse Problems*, 24(1):015016, 2008.

[57] Panagiotis Michaleris, Daniel A. Tortorelli, and Creto A. Vidal. Tangent operators and design sensitivity formulations for transient non-linear coupled problems with applications to elastoplasticity. *International Journal for Numerical Methods in Engineering*, 37(14):2471–2499, 1994.

[58] Biaosong Chen and Liyong Tong. Thermomechanically coupled sensitivity analysis and design optimization of functionally graded materials. *Computer Methods in Applied Mechanics and Engineering*, 194(18-20):1891–1911, 2005.

[59] Yixian Du, Zhen Luo, Qihua Tian, and Liping Chen. Topology optimization for thermo-mechanical compliant actuators using mesh-free methods. *Engineering Optimization*, 41(8):753–772, 2009.

[60] Shiguang Deng and Krishnan Suresh. Stress constrained thermo-elastic topology optimization with varying temperature fields via augmented topological sensitivity based level-set. *Structural and Multidisciplinary Optimization*, 56(6):1413–1427, 2017.

[61] T. Shibukawa, V. D. Gupta, R. Turner, J. H. Dillon, and A. V. Tobolsky. Temperature Dependence of Shear Modulus and Density of Nylon-6. *Textile Research Journal*, 32(12):1011–1012, 1962.

[62] Douglas C. Hopkins, Theodore Baltis, James M. Pitaress, and Donald R. Hazelmyer. Extreme Thermal Transient Stress Analysis with Pre-Stress in a Metal Matrix Composite Power Package. *Additional Conferences (Device Packaging, HiTEC, HiTEN, & CICMT)*, 2012(HITEC):000361–000372, 2012.

[63] Leon Govaert, Brian Brown, and Paul Smith. Temperature dependence of the Young's modulus of oriented polyethylene. *Macromolecules*, 25(13):3480–3483, 1992.

[64] Krister Svanberg. The method of moving asymptotes—a new method for structural optimization. *International Journal for Numerical Methods in Engineering*, 24(2):359–373, 1987.

[65] Tyler E. Bruns and Daniel A. Tortorelli. Topology optimization of non-linear elastic structures and compliant mechanisms. *Computer Methods in Applied Mechanics and Engineering*, 190(26-27):3443–3459, 2001.

[66] Ole Sigmund. Morphology-based black and white filters for topology optimization. *Structural Multidisciplinary Optimization*, 33:401–424, 2007.

[67] Erik Andreassen, Anders Clausen, Mattias Schevenels, Boyan S. Lazarov, and Ole Sigmund. Efficient topology optimization in MATLAB using 88 lines of code. *Structural and Multidisciplinary Optimization*, 43(1):1–16, 2011.

[68] J. K. Guest, J. H. Prévost, and T. Belytschko. Achieving minimum length scale in topology optimization using nodal design variables and projection functions. *International Journal for Numerical Methods in Engineering*, 61(2):238–254, 2004.

[69] Ole Sigmund. On the usefulness of non-gradient approaches in topology optimization. *Structural and Multidisciplinary Optimization*, 43(5):589–596, 2011.

[70] T. Liszka and M. Ostoja-Starzewski. Effects of microscale material randomness on the attainment of optimal structural shapes. *Structural and Multidisciplinary Optimization*, 26(1-2):67–76, 2004.

[71] P. G. Coelho and H. C. Rodrigues. Hierarchical topology optimization addressing material design constraints and application to sandwich-type structures. *Structural and Multidisciplinary Optimization*, 52(1):91–104, 2015.

[72] Joe Alexandersen, Niels Aage, Casper Schousboe Andreasen, and Ole Sigmund. Topology optimisation for natural convection problems. *International Journal for Numerical Methods in Fluids*, 76(10):699–721, 2014.

[73] Joe Alexandersen, Ole Sigmund, and Niels Aage. Large scale three-dimensional topology optimisation of heat sinks cooled by natural convection. *International Journal of Heat and Mass Transfer*, 100:876–891, 2016.

[74] Younghwan Joo, Ikjin Lee, and Sung Jin Kim. Topology optimization of heat sinks in natural convection considering the effect of shape-dependent heat transfer coefficient. *International Journal of Heat and Mass Transfer*, 109:123–133, 2017.

[75] Shutian Liu, Quhao Li, Junhuan Liu, Wenjiong Chen, and Yongcun Zhang. A Realization Method for Transforming a Topology Optimization Design into Additive Manufacturing Structures. *Engineering*, 4(2):277–285, 2018.